

UNCOVER/MegaScience: No Evidence of Environmental Quenching in a $z \sim 2.6$ Proto-cluster

RICHARD PAN,¹ KATHERINE A. SUESS,² DANILO MARCHESINI,¹ BINGJIE WANG (王冰洁),^{3,4,5} JOEL LEJA,^{3,4,5} SAM E. CUTLER,⁶
KATHERINE E. WHITAKER,^{6,7} RACHEL BEZANSON,⁸ SEDONA H. PRICE,⁸ LUKAS J. FURTAK,⁹ JOHN R. WEAVER,⁶ IVO LABBÉ,¹⁰
GABRIEL BRAMMER,⁷ YUNCHONG ZHANG,⁸ PRATIKA DAYAL,¹¹ ROBERT FELDMANN,¹² KARL GLAZEBROOK,¹³ JENNY E. GREENE,¹⁴
TIM B. MILLER,¹⁵ IKKI MITSUHASHI,² THEMIYA NANAYAKKARA,¹⁰ ERICA J. NELSON,² DAVID J. SETTON,^{14,*} AND ADI ZITRIN⁹

¹*Department of Physics & Astronomy, Tufts University, Medford, MA 02155, USA*

²*Department for Astrophysical and Planetary Science, University of Colorado, Boulder, CO 80309, USA*

³*Department of Astronomy & Astrophysics, The Pennsylvania State University, University Park, PA 16802, USA*

⁴*Institute for Computational & Data Sciences, The Pennsylvania State University, University Park, PA 16802, USA*

⁵*Institute for Gravitation and the Cosmos, The Pennsylvania State University, University Park, PA 16802, USA*

⁶*Department of Astronomy, University of Massachusetts, Amherst, MA 01003, USA*

⁷*Cosmic Dawn Center (DAWN), Niels Bohr Institute, University of Copenhagen, Jagtvej 128, København N, DK-2200, Denmark*

⁸*Department of Physics and Astronomy and PITT PACC, University of Pittsburgh, Pittsburgh, PA 15260, USA*

⁹*Physics Department, Ben-Gurion University of the Negev, P.O. Box 653, Be'er-Sheva 84105, Israel*

¹⁰*Centre for Astrophysics and Supercomputing, Swinburne University of Technology, Melbourne, VIC 3122, Australia*

¹¹*Kapteyn Astronomical Institute, University of Groningen, 9700 AV Groningen, The Netherlands*

¹²*Department of Astrophysics, University of Zurich, Zurich CH-8057, Switzerland*

¹³*Centre for Astrophysics and Supercomputing, Swinburne University of Technology, PO Box 218, Hawthorn, VIC 3122, Australia*

¹⁴*Department of Astrophysical Sciences, Princeton University, 4 Ivy Ln., Princeton, NJ 08544, USA*

¹⁵*Center for Interdisciplinary Exploration and Research in Astrophysics (CIERA), Northwestern University, 1800 Sherman Ave, Evanston IL 60201, USA*

(Received XXX; Revised XXX; Accepted XXX)

Submitted to the Astrophysical Journal Letters

ABSTRACT

Environmental quenching – where interactions with other galaxies and/or the intra-cluster medium (ICM) suppress star formation in low-mass galaxies – has long been proposed as the primary driver to establish the red sequence for low-mass galaxies within clusters at low redshift ($z < 1$). However, we still do not know whether these environmental quenching mechanisms are also active at higher redshifts in proto-cluster environments that have yet to fully virialize. In large part, this regime has remained unexplored due to observational limitations; however, the James Webb Space Telescope has recently opened a new window into the role of environmental quenching on low-mass ($\log(M_*/M_\odot) < 9.5$) galaxies at cosmic noon ($2 < z < 3$). Here, we use data from the JWST UNCOVER and MegaScience programs to directly probe the role of environmental quenching on low-mass galaxies in a newly-discovered $z \approx 2.6$ overdensity. Leveraging the deep imaging and $R \sim 15$ spectrophotometry enabled by these JWST/NIRCam data, we analyze the stellar populations and inferred star formation histories (SFHs) of 20 low-mass ($8.5 < \log(M_*/M_\odot) \leq 9.0$) quiescent galaxies in the overdense environment and compare to a similar sample of 18 such galaxies in the field. The SFHs of quiescent galaxies in the proto-cluster and field across the entire probed stellar mass regime ($8.5 < \log(M_*/M_\odot) \leq 11.0$) are indistinguishable, demonstrating that the environment at cosmic noon is not yet accelerating quenching compared to the field. This is consistent with expectations that proto-clusters at $z > 2$ have yet to virialize and develop a dense enough environment to efficiently quench low-mass galaxies.

Keywords: Galaxy evolution (594); Galaxy structure (622); Galaxy quenching (2040); Galaxy environments (2029); Extragalactic astronomy (506); Protoclusters (1297); James Webb Space Telescope (2291)

1. INTRODUCTION

Nothing lasts forever. For many galaxies, their star formation shuts down, often referred to as “quenching”. How these quiescent galaxies quenched and what the primary quenching mechanisms are across different stellar mass and redshift regimes are not yet fully understood (Man & Belli 2018). Different mechanisms have been proposed to quench galaxies and are roughly separated into internal and external processes (Peng et al. 2010b). Internal processes include quenching via stellar winds, supernovae feedback, and AGN feedback (Ciotti et al. 1991; Croton et al. 2006; Ishibashi & Fabian 2012; Man & Belli 2018). External processes, commonly known as environmental quenching, include quenching via ram-pressure stripping, galaxy interactions, strangulation, and harassment, and primarily affect low stellar mass galaxies (Gunn & Gott 1972; Farouki & Shapiro 1981; Moore et al. 1996; Balogh et al. 2004; Peng et al. 2015; Alberts & Noble 2022).

Environmental processes have been seen to drive lower-mass ($\log(M_*/M_\odot) < 10$) galaxies to quench, building up the red sequence in lower redshift ($z \leq 1.5$) clusters (Dressler 1980; Balogh et al. 2004; Kauffmann et al. 2004; Baldry et al. 2006; Peng et al. 2010b; Muzzin et al. 2014; Kawinwanichakij et al. 2017; Tomczak et al. 2017; Papovich et al. 2018; van der Burg et al. 2020). A key driver of this buildup is the hot ICM, which can quench infalling galaxies by stripping away their cold gas through ram-pressure stripping on rapid timescales or preventing further gas accretion, leading to galaxy strangulation on longer timescales (Sarazin 1986; Cowl & Kenney 2008; Muzzin et al. 2014; Boselli & Gavazzi 2014; Peng et al. 2015; Steinhauser et al. 2016; Chiang et al. 2017; Rodríguez Montero et al. 2019; Cortese et al. 2021; Boselli et al. 2022; Alberts & Noble 2022). The assumption is that low-mass quiescent galaxies in dense galaxy clusters would be still forming stars if they lived in a less dense environment. Instead their star formation is truncated early due to these environmental processes, resulting in systematically older stellar populations compared to similar-mass galaxies in the field (Trager et al. 2000; van Dokkum & Stanford 2003; Thomas et al. 2005; Renzini 2006; Thomas et al. 2010; Paulino-Afonso et al. 2020). This age discrepancy reflects a greater efficiency of environmental quenching mechanisms in clusters, which also contribute to a higher “quenched fraction” – the fraction of all galaxies that are quiescent for a given stellar mass range – in overdensities compared to the field (Tomczak et al. 2017; Papovich et al. 2018; McNab et al. 2021; Forrest et al. 2024).

While these mechanisms are at play at lower redshift, it is unclear whether we would expect them to have a large effect at cosmic noon and beyond. Galaxy clusters undergo a major transition between $1.5 < z \leq 5.0$, going from dynamically evolving, unvirialized proto-cluster structures towards virialized clusters in hydrostatic equilibrium (Chiang et al. 2017). During this transition epoch, proto-clusters are forming the bulk of their total stellar mass ($\sim 65\%$), undergoing virialization leading to stable equilibrium, and assembling smaller dark-matter halos onto the central halo as they develop their hot ICM (Sarazin 1986; Chiang et al. 2013; Muldrew et al. 2015; Overzier 2016; Chiang et al. 2017; Alberts & Noble 2022). To date, most studies of proto-clusters at cosmic noon have only been able to examine higher-mass galaxies ($\log(M_*/M_\odot) > 9.5$), due to difficulty with observing faint low-mass galaxies at large cosmic distances (Kawinwanichakij et al. 2016, 2017; Tomczak et al. 2017; van der Burg et al. 2020; Edward et al. 2024; Forrest et al. 2024; Singh et al. 2024). These studies have found that between $2.0 < z < 3.5$, the quenched fractions remain similar across environments, suggesting environmental quenching has a minor role in building the red sequence at $\log(M_*/M_\odot) > 9.5$ (Edward et al. 2024; Forrest et al. 2024).

So the question is: can proto-cluster environments efficiently quench low-mass galaxies ($\log(M_*/M_\odot) < 9.5$) even before they undergo this big transition, or can only fully virialized massive clusters drive environmental quenching of low-mass galaxies? Until JWST, the lower mass quiescent population at cosmic noon was below the observational detection limit of even the Hubble Space Telescope (Tal et al. 2014). Since then, JWST has dramatically opened up new windows on the population of low-mass quiescent galaxies at cosmic noon, both through photometric (Cutler et al. 2024; Hamadouche et al. 2024; Alberts et al. 2024) and spectroscopic (Marchesini et al. 2023) studies. Yet, a comprehensive analysis of low-mass quiescent galaxies in overdensities has been limited by the lack of detailed spectral energy distribution (SED) sampling in the rest-frame near-infrared, crucial for accurately constraining galaxy stellar populations due to its sensitivity to the bulk of stellar mass (Bell & de Jong 2001).

In this Letter, we present a serendipitously discovered $z \approx 2.58$ proto-cluster candidate behind the Abell 2744 lensing field. We use data from the JWST Ultradeep NIRSpect and NIRCams Observations before the Epoch of Reionization (UNCOVER) Cycle 1 Treasury Program (Bezanson et al. 2024) and the Medium Bands, Mega Science Cycle 2 survey (Suess et al. 2024). We leverage the unprecedented depth (~ 29.5 AB to ~ 32.0 AB with magnification; Weaver et al. 2024) and the constraining power of the NIRCams medium band photometry ($\sigma_{\text{NMAD}} \sim 0.01$; Suess et al. 2024) to robustly infer the redshifts and stellar populations (Wang et al.

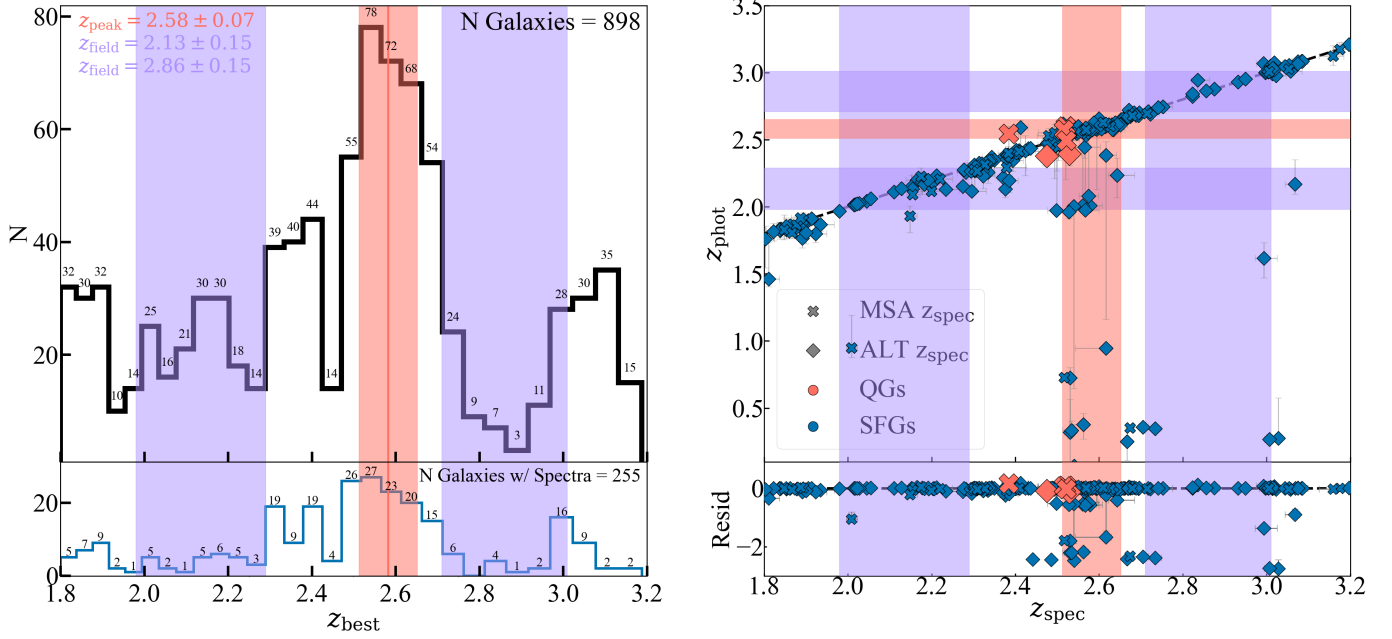


Figure 1. Top left: Redshift histogram of all galaxies in the redshift range centered around cosmic noon adopting the “best” available redshift as detailed in section 2.1. Bottom left: Redshift histogram of all galaxies with spectroscopic redshifts from the UNCOVER DR4 redshift catalog (Price et al. 2024) and the ALT DR1 catalog (Naidu et al. 2024). The overdensity is centered at $z \approx 2.58$ (red) while the field was selected at higher and lower redshifts. Right: Comparison of photometric and spectroscopic redshifts of 255 galaxies with the bottom right panel being the residual of the two ($z_{\text{phot}} - z_{\text{spec}}$). Quiescent and star-forming galaxies are indicated by red and blue symbols while MSA and GRISM objects are indicated by crosses and diamonds. The red and purple stripes denote the overdensity and field redshift ranges. Our $\sigma_{\text{NMAD}} \approx 0.01$ is consistent with a $\sigma_{\text{NMAD}} \approx 0.015$ found in Suess et al. (2024) and highlights the constraining power of the medium band photometry.

2024). This allows us to identify proto-cluster candidates and their low-mass quiescent members of which we find 218 likely proto-cluster members including 34 quiescent galaxies. We compare their stellar populations and morphologies to those of their field counterparts (228 members and 29 quiescent galaxies), exploring, for the first time, the effects of the environment on the SFHs of low-mass galaxies at cosmic noon. All magnitudes are given in the AB system and a WMAP9 cosmology (Hinshaw et al. 2013) with $H_0 = 69.32 \text{ km s}^{-1} \text{ Mpc}^{-1}$, $\Omega_M = 0.2865$, and $\Omega_\Lambda = 0.7135$, along with a Chabrier (2003) initial mass function.

2. METHODS

2.1. Data

We use the DR3 photometric catalog from the UNCOVER (JWST-GO-2561, PIs: Bezanson & Labbé; Bezanson et al. 2024) and MegaScience (JWST-GO-4111, PI: Suess; Suess et al. 2024) surveys. The dataset contains all 20 NIR-Cam broad- and medium-band filters, including data from GLASS-ERS (Treu et al. 2022), ALT (PIs: Matthee & Naidu; Naidu et al. 2024), MAGNIF (PI: Sun; Li et al. 2023), GO-3538 (PI: Iani), and GO-2756 (PI: Chen; Chen et al. 2024). We also utilize HST data in F435W, F606W, F814W, F105W, F140W, and F160W from the HFF (Lotz et al. 2017) and BUFFALO (Steinhardt et al. 2020) programs. The catalog construction is detailed in Weaver et al. (2024).

When available we include spectroscopic redshifts (z_{spec}) in place of photometric redshifts (z_{phot}). The spec- z s are provided by the UNCOVER DR4 spectroscopic redshift catalog (Price et al. 2024) and the ALT DR1 redshift catalog (Naidu et al. 2024). The UNCOVER NIRSpc/MSA follow-up survey targeted ~ 700 objects in A2744 and the reduction was done using MSAEXP as part of the GRIZLI data reduction pipeline (Brammer et al. 2008). Of these, ~ 330 objects have secure spec- z s ($\text{flag_zspec_qual} > 2$; two or more secure spectral features) which we use in place of their photo- z s. For survey design and detailed reductions, please refer to Price et al. (2024). The ALT DR1 catalog provides NIRC/GRISM redshifts for 1630 sources between $0.2 < z \leq 8.5$ (Naidu et al. 2024). When incorporating the “best” redshifts (z_{best}), we first adopt spectroscopic redshifts from the UNCOVER catalog. When these are unavailable, we use the GRISM redshifts from the ALT catalog. If neither is available, we use the best-fit photometric redshifts as described below.

We fit the photometry to derive galaxy properties using the PROSPECTOR- β model from Wang et al. (2023), which uses the PROSPECTOR Bayesian inference framework (Johnson et al. 2021). The PROSPECTOR- β model robustly infers the redshift, rest-frame colors, and stellar population synthesis (SPS) properties such as stellar masses and SFHs (Wang et al. 2023). We adopt v2.0 of the parametric

strong lensing model of A2744 by [Furtak et al. \(2023\)](#), which was recently updated with UNCOVER spectroscopic redshifts in [Price et al. \(2024\)](#), to compute magnification factors and correct the flux when fitting for the redshift and SPS properties. When possible, we fix the galaxy redshift at its spectroscopic redshift in the PROSPECTOR modeling. All data products for UNCOVER and MegaScience are accessible on the UNCOVER survey web page, <https://jwst-uncover.github.io/DR3.html> and Zenodo (doi: 10.5281/zenodo.8199802, doi: 10.5281/zenodo.14559840, and doi: 10.5281/zenodo.14281664).

2.2. Sample Selection

We search for overdensities in redshift space to identify proto-cluster candidates. We select an initial sample of galaxies around cosmic noon with `USE_PHOT=1` flag (see [Weaver et al. 2024](#)), $\log(M_*/M_\odot) > 8.5$, $1.8 < z < 3.2$, and filter coverage within the footprint of the MegaScience survey (see [Suess et al. 2024](#) for a detailed footprint). All galaxies in this mass-selected sample have $m_{F444W} < 26.5$ AB, making them significantly brighter than the F444W 5σ point-source detection limit (28.24 AB; [Weaver et al. 2024](#)) and indicating that our sample is well within the mass-complete regime. This initial sample ensures that the galaxies' SEDs are sampled by all broad- and medium-bands over the deepest region of observation, resulting in the most accurate photo- z s.

To quantify the accuracy of our photometric redshifts in this regime, we compare the photo- z s with the spec- z s of sources. In the right panel of Figure 1, we present the performance from our PROSPECTOR photo- z s against the UNCOVER and ALT spec- z s in the range $1.8 < z < 3.2$. We find a NMAD ([Brammer et al. 2008](#); [Weaver et al. 2024](#)) of $\sigma_{\text{NMAD}} \approx 0.01$ in this redshift slice, which is comparable to the NMAD found by [Suess et al. \(2024\)](#) ($\sigma_{\text{NMAD}} \approx 0.015$) over the entire sample. We note that the extreme photo- z outliers (e.g., $z_{\text{phot}} \sim 0.5$ to $z_{\text{spec}} \sim 2.6$) are examples of featureless high- z continua misidentified as low- z quiescent galaxies. See [Cutler et al. \(in prep.\)](#) for further detail on identifying low- z cluster quiescent galaxies.

We plot the redshift distribution of galaxies from this initial sample (left panel in Figure 1) and identify an overdensity peak at $z = 2.58 \pm 0.07$. We define the uncertainty of our redshift ranges, $\sigma = \pm 0.07$, as approximately two times the typical uncertainty of our sample ($\Delta z \approx 0.033$). This yields an overdensity range between $2.51 < z < 2.65$ totaling 217 galaxies. We note that this redshift overdensity is detected in the ALT survey from H α and Pa γ emission at $z \approx 2.56$, fully consistent with our photometric findings ([Naidu et al. 2024](#)).

The main goal of this paper is to compare the SFHs of galaxies in this overdensity and the coeval field. This requires a field comparison sample that is close in redshift to

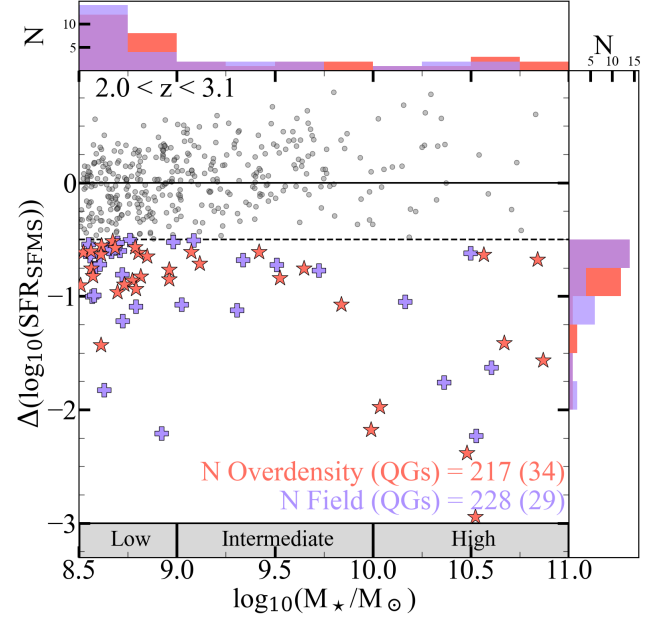


Figure 2. We select quiescent galaxies by the relative difference, $\Delta \log_{10}(\text{SFR}_{\text{SFMS}})$, between their $\log_{10}(\text{SFR}_{100})$ and the SFMS at their redshift from [Leja et al. \(2022\)](#) as a function of stellar mass. Quiescent galaxies are selected to be at least 0.5 dex below (dashed curve) the main-sequence of star-forming galaxies from [Leja et al. \(2022\)](#) (solid curve). Quiescent galaxies in the overdensity and in the field are shown as red stars and purple crosses, respectively. As shown in the histograms in the top and right panels, we find that the two subsamples are distributed similarly.

the candidate overdensity at $z \sim 2.58$. We avoid $z \approx 2.4$ and $z \approx 3.1$, which from the left panel of Figure 1 may also represent slightly overdense environments. Given this constraint, we select two redshift windows above and below the overdensity that yields a similar number of members. This leads to two redshift ranges centered at $z = 2.13 \pm 0.15$ and $z = 2.86 \pm 0.15$ roughly corresponding to ± 400 Myr of the overdensity and yielding 228 field galaxies. Averaging over a higher- and lower-redshift bin helps mitigate any potential environmental effects from the age of the universe. Our conclusions in this work do not vary with small redshift range changes for the overdensity and field.

Next, we select quiescent galaxies as all galaxies with derived star-formation rates, averaged over the last 100 Myr (SFR_{100}), more than 0.5 dex below the main-sequence of star-forming galaxies (SFMS) at a given epoch from [Leja et al. \(2022\)](#). We note that at $z \approx 2.7$ the main sequence of star-forming galaxies from [Leja et al. \(2022\)](#) only extends to $\log(M_*/M_\odot) > 10.2$. Therefore we extrapolate this selection to lower masses ($\log(M_*/M_\odot) > 8.5$). This extrapolation is well-motivated by previous studies which have found that the slope of the main sequence is constant down to lower masses, likely because the physics of star formation does not dramatically differ below $\log(M_*/M_\odot) < 10.2$ ([Whitaker et al.](#)

2014; Leja et al. 2022; Mérida et al. 2023). An alternative method for selecting low-mass quiescent galaxies is to use a rest-frame $U - V$ vs $V - J$ color-color selection (UVJ diagram) without the $U - V$ lower limit cut (Belli et al. 2019; Alberts et al. 2024; Cutler et al. 2024), as proposed by Belli et al. (2019). Such a cut would allow for the selection of younger and lower-mass quiescent galaxies coming out of a star-burst phase with bluer $U-V$ colors (Alberts et al. 2024). We test our selection and find similar results whether we use a SFR or a UVJ cut to select quiescent galaxies.

Figure 2 shows our full sample of galaxies (218 in the overdensity, 228 in the field) as well as our quiescent subsample (34 in the overdensity, and 29 in the field). Marginal histograms show the distributions of our quiescent overdensity and field sample; the two samples have similar stellar mass and SFR distributions despite their small difference in redshift.

Throughout the rest of this Letter, we split our quiescent sample into three regimes of stellar mass: low-mass ($8.5 < \log(M_*/M_\odot) \leq 9.0$), intermediate-mass ($9.0 < \log(M_*/M_\odot) \leq 10.0$), and high-mass ($10.0 < \log(M_*/M_\odot) \leq 11.0$). We find $N = 20$ (18) low-mass, 7 (6) intermediate-mass, and 7 (5) high-mass overdensity (field) quiescent galaxies. In total, our quiescent sample includes 34 galaxies in the overdensity and 29 galaxies in the field.

2.3. Formation and Quenching Times

To quantify potential differences in the stellar populations of proto-cluster members and field members, we calculate the formation and quenching times of our quiescent galaxies from their PROSPECTOR SFHs, which were derived from SED fitting to the 20-band photometry. We define the formation time as the lookback time when a galaxy formed 50% of its total mass, t_{50}^{lb} . We consider the quenching time as the lookback time when a galaxy formed 90% of its total mass, t_{90}^{lb} . Lastly, we establish the quenching timescale to be the difference of the two ($\Delta t = t_{50}^{\text{lb}} - t_{90}^{\text{lb}}$), roughly indicating “how long it took to quench”. The PROSPECTOR framework uses the DYNESTY dynamic nested sampling package (Speagle 2020) to sample draws from the prior distribution (Johnson et al. 2021). We calculate t_{50}^{lb} , t_{90}^{lb} , and Δt from each draw in the PROSPECTOR fit and report the 50th percentile of the resulting posterior as the best-fit value and the 16-84th percentile as the 1σ error bar. Our focus is to compare these timescales relative to each other (i.e., overdensity versus field). We refrain from drawing comparisons to other observational studies that made different prior assumptions on the SFHs given the large impact certain prior choices can have on these derived quantities (Leja et al. 2019; Suess et al. 2022).

3. ANALYSIS

If the proto-cluster environment at cosmic noon is affecting the quenching mechanisms of galaxies then we might see differences in the SFHs of quiescent galaxies in the overdensity against the field as seen in lower-redshift clusters (Trager et al. 2000; van Dokkum & Stanford 2003; Thomas et al. 2005; Renzini 2006; Thomas et al. 2010; Paulino-Afonso et al. 2020). We present the comparisons of the SFH timescales and SFHs in Figure 3. The left column compares t_{50}^{lb} and t_{90}^{lb} of quiescent galaxies in the overdensity and field across three stellar mass bins, while the middle column examines quenching timescales as a function of redshift. We use a two sample Kolmogorov-Smirnov (KS) test to compare the distributions of median SFH times and timescales between environments. The p-values for t_{50}^{lb} are 0.12, 0.09, and 0.84, for t_{90}^{lb} are 0.26, 0.07, and 0.33, and for Δt are 0.13, 0.09, and 0.33, corresponding to low-, intermediate-, and high-mass bins. All p-values are greater than 0.05, indicating that we cannot reject the hypothesis that the overdensity and field samples are drawn from the same parent population. The right column illustrates the stacked SFHs of galaxies in the overdense environment versus those in the field. The SFHs are indistinguishable within 1σ , suggesting no significant difference between quiescent galaxies in the overdensity and the field. This finding further supports the results from the KS tests.

3.1. Bayesian Population Modeling

The KS tests provide a comparison of the median distributions of galaxies in the overdensity and the field, but do not account for uncertainties in individual measurements of t_{50}^{lb} , t_{90}^{lb} , and Δt . To incorporate these uncertainties, we use a Bayesian population modeling framework to infer the underlying population distributions while propagating measurement errors, following the method of Leja et al. (2020). This approach allows us to compare the full posterior distributions of all galaxies collectively, rather than relying solely on median values.

We model the distributions of t_{50}^{lb} , t_{90}^{lb} , and Δt for quiescent galaxies as Gaussian functions, leaving the mean and standard deviation of each Gaussian as a free parameter. We separate the data into 3 mass bins (low-, intermediate-, and high-mass), 2 environments (overdensity and field), and 3 SFH timescales (t_{50}^{lb} , t_{90}^{lb} , and Δt) totaling 18 models. The distributions are represented as such:

$$G(x) = \frac{1}{\sigma\sqrt{2\pi}} e^{-0.5\left(\frac{x - \mu_{\text{pop}}}{\sigma_{\text{pop}}}\right)^2} \quad (1)$$

where μ_{pop} and σ_{pop} represent the population mean and dispersion. The observations, x , consist of t_{50}^{lb} , t_{90}^{lb} , and Δt values for N galaxies. In contrast to the KS tests above, which only use a single value for each galaxy (the posterior me-

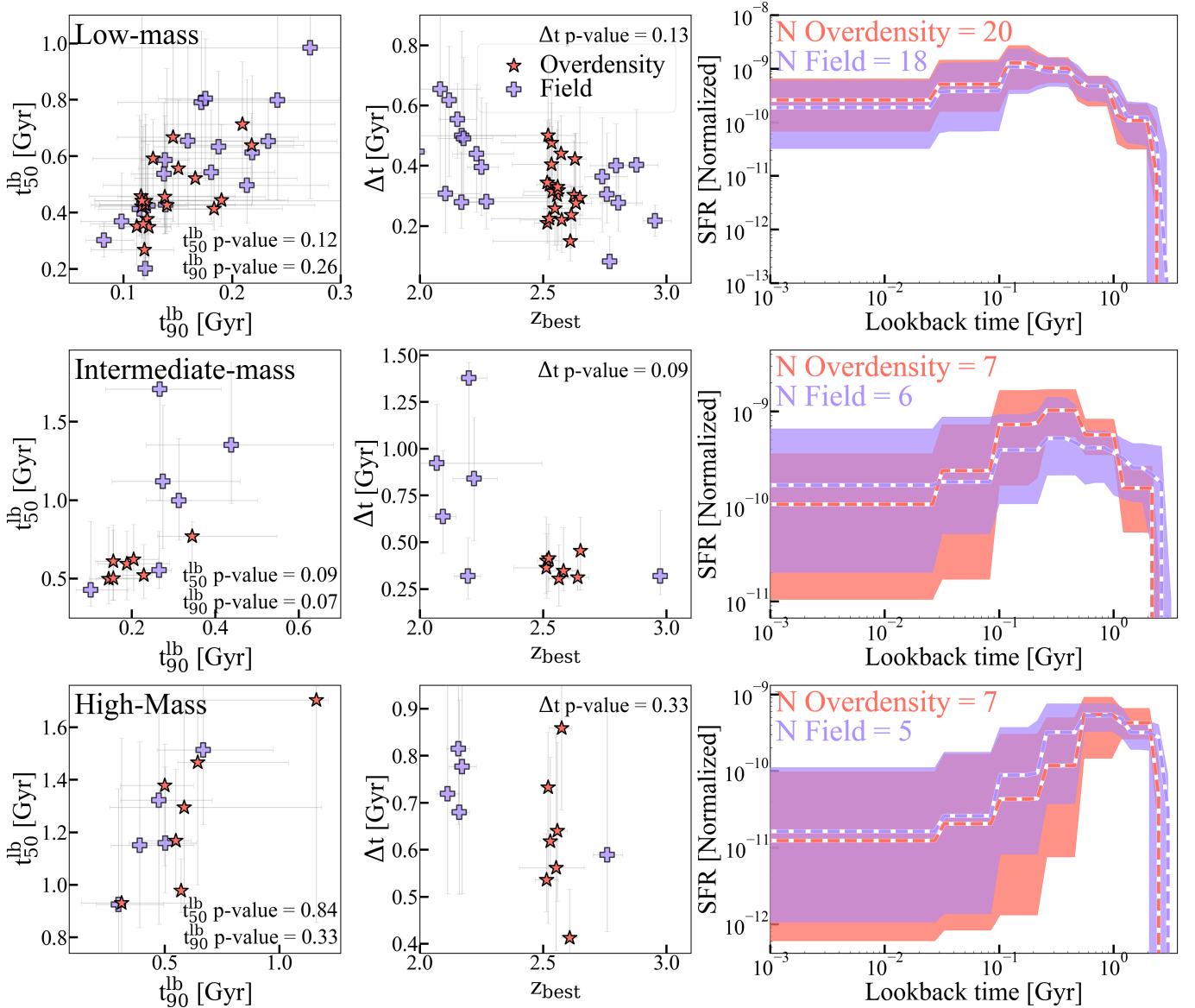


Figure 3. Left: Comparison of the formation time (t_{50}^{lb}) and the quenching time (t_{90}^{lb}) in three stellar mass bins: low-mass ($8.5 < \log(M_*/M_\odot) \leq 9.0$), intermediate-mass ($9.0 < \log(M_*/M_\odot) \leq 10.0$), and high-mass ($10.0 < \log(M_*/M_\odot) \leq 11.0$). Middle: Comparison of the Δt timescale versus the redshift in the same stellar mass bins. Right: Stacked SFHs of the overdensity and field galaxies in the same stellar mass bins. The shaded regions indicate the 1σ uncertainty while the dashed lines indicate the median SFHs. We compare the distributions in the left and middle panels using a KS test and find them to be statistically indistinguishable. Similarly, the stacked SFHs in the right panels are consistent within 1σ demonstrating similar quenching pathways irrespective of environment.

dian), this method incorporates all 1000 posterior draws for each galaxy. The likelihood of observing a single galaxy is computed as the average likelihood over its 1000 draws. The total log-likelihood, $\ln(P)$, for all N galaxies is given by:

$$\ln(P) \approx \sum_{i=1}^N \ln \left(\frac{\sum_{j=1}^M g(x_{i,j})}{M} \right) \quad (2)$$

Before fitting, we set uniform priors on our fit parameters, μ_{pop} and σ_{pop} , of each stellar mass bin and environment. The prior range for μ_{pop} is set by the minimum and maxi-

mum observed values, ensuring that the population mean lies within the observed data range. For σ_{pop} , we use a lower bound of u , the typical measurement uncertainty in each bin, as values below this are indistinguishable from measurement noise. The upper bound is set to 2 Gyrs, which is sufficiently large enough given the age of the universe at our upper limit, $z = 3.0$ (~ 2.1 Gyr).

We perform mock recovery tests to assess the accuracy of our population modeling. We generate N mock galaxy observations sampled from a normal distribution with a fixed μ_{pop} and varying σ_{pop} , producing a distribution of observed

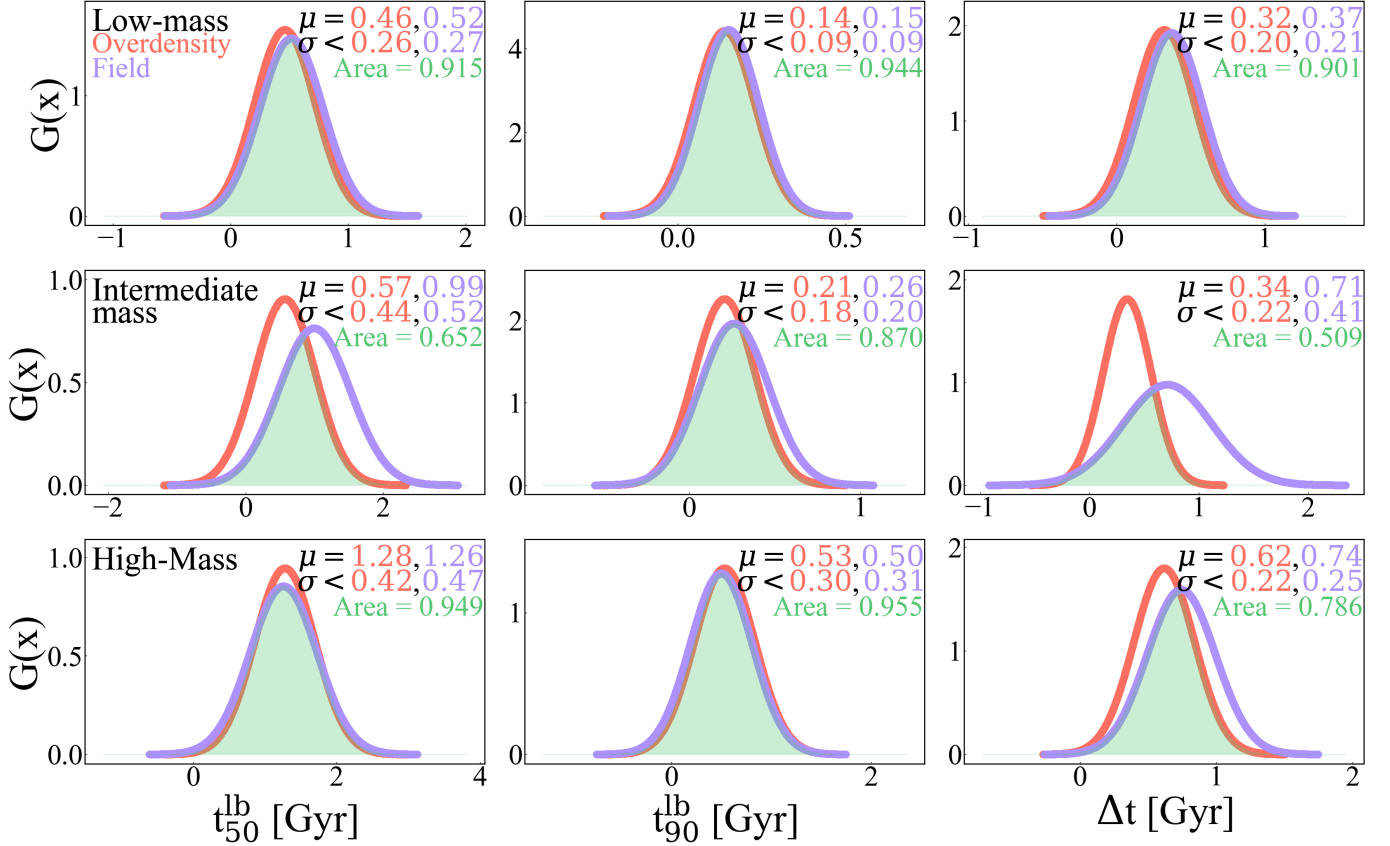


Figure 4. We show the best-fit population models centered at the mean, μ , with a dispersion of σ . The columns are a comparison of t_{50}^{lb} , t_{90}^{lb} , and Δt while the rows are a comparison of the different stellar mass regimes from top to bottom, low-mass intermediate-mass, and high-mass. The population distribution of the overdensity is colored in red while the field is in purple. The overlapping area below the two distributions is in green which roughly quantifies the similarity of the two populations. There is significant overlap between the population models of the overdensity and field indicating similar SFH timescales between the two.

means, μ_{obs} . For each mock galaxy, we generate 1000 mock draws by sampling a normal distribution with $\mu = \mu_{\text{obs}, n}$, and $\sigma = u$. The number of galaxies, N , is varied between 5 and 20, matching our sample sizes. Our tests show that μ_{pop} is accurately recovered within 1σ for any input σ_{pop} and u . However, σ_{pop} is not well recovered for $\sigma_{\text{pop}} < u$, as the recovered dispersion remains at u , indicating that measurement noise and intrinsic dispersion are indistinguishable below this threshold. Thus we set the lower bound of σ_{pop} to be u , preventing the model from inferring an intrinsic dispersion below where it becomes indistinguishable from measurement noise. Lastly, the best-fit recovered μ_{pop} and σ_{pop} remains unchanged with varying N and their uncertainties decrease as the sample size increases. These tests ensure the robustness of our modeling, allowing us to draw reliable conclusions about the population properties of these samples.

Figure 4 presents the results of our Bayesian population modeling in which we compare the population distributions of the overdensity and field across stellar mass bins (rows) and SFH timescales (columns). We find that the population models of quiescent galaxies in the overdensity and the field

are quite similar, with a typical overlapping area $\geq 75\%$. The largest difference occurs in the intermediate-mass bin for Δt (area = 50.9%) in which the overdensity quiescent galaxies may have slightly shorter quenching timescales. The Δt distributions for intermediate-mass overdensity galaxies and field galaxies ($\mu_{\text{pop}} = 0.34$, $\sigma_{\text{pop}} = 0.22$ and $\mu_{\text{pop}} = 0.71$, $\sigma_{\text{pop}} = 0.41$ respectively) do differ as is also the case for t_{50}^{lb} (middle left panel in Figure 4). However, these differences are within 2σ and may not indicate large intrinsic differences in the populations, especially when considering the uneven distribution of field galaxies (1 galaxy in the higher redshift intermediate mass field bin; central panel in Figure 3). Confirming this potential difference requires further analysis with larger samples, a truly coeval field sample, and more precise age measurements to constrain the population distribution.

Overall, these results support the KS test results that the SFHs of quiescent galaxies in overdense and field environments at $z \sim 2.6$ are statistically indistinguishable across the stellar mass range $8.5 < \log(M_*/M_\odot) \leq 11.0$.

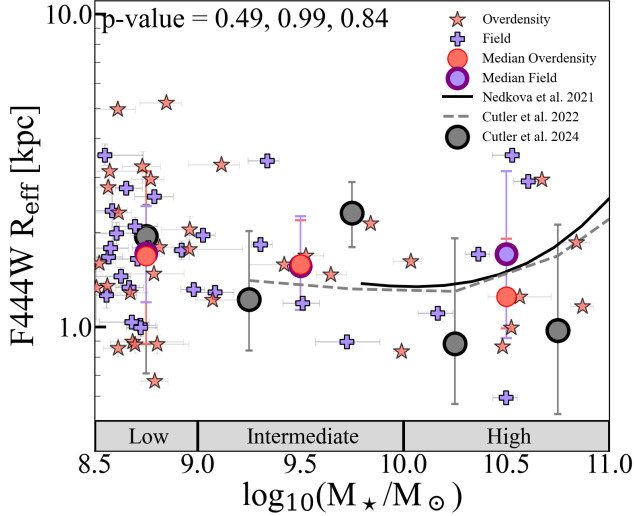


Figure 5. Mass-size relation of quiescent galaxies in the overdensity (red stars) and the field (blue crosses), measured in the JWST NIRCcam F444W. Their median mass-size are shown as red and blue circles, respectively, along with median values from Cutler et al. (2024) (grey circles). We also overplot the mass-size relation from HST F160W measurements from Nedkova et al. (2021) (solid black) and Cutler et al. (2022) (dashed black). We find a similarly flat mass-size relation and no significant difference between the overdensity and field populations.

3.2. Sizes

Lastly, we investigate the sizes of the two populations to see whether the overdense environment has affected their structural properties as seen in previous work (Kuchner et al. 2017; Carlsten et al. 2021). We use PYSERVIC, a Bayesian inference fitting tool (Pasha & Miller 2023), to fit 1D Sérsic profiles to the F444W images. In this redshift regime, F444W probes rest-frame $\sim 1.2 \mu m$ where we expect the light to trace the stellar mass distribution of galaxies (Bell & de Jong 2001). The methods are described in detail in Zhang et al. (in prep.) and Miller et al. (2024). In brief, we simultaneously fit all other sources within 2 arcsecs of the main object, within 2 magnitudes in F277W, F356W, and F444W of the main objects, and a SNR > 5 in F277W, F356W, and F444W. We mask any other sources in the UNCOVER DR3 segmentation map. We draw samples from the posterior using a No U-turn sampler using 2 chains with 750 warm-up and 500 sampling steps each (Hoffman & Gelman 2014; Phan et al. 2019).

We show the mass-size relation in Figure 5 with the circular scatter points illustrating the median effective radii (semi-major axis) in a given stellar mass bin. We perform a KS test in each stellar mass bin comparing the sizes of quiescent galaxies in the overdensity and those in the field. Because of the large p-values of 0.49, 0.99, and 0.84 (low-, intermediate-, high-mass), we reject the hypothesis that the overdense and field samples are drawn from the same parent population.

Our median results are similar to size measurements from Nedkova et al. (2021) (HST F160W), Cutler et al. (2022) (HST F160W) and Cutler et al. (2024) (JWST F444W), all of which use the GALFIT fitting tool (Peng et al. 2002, 2010a) and measure primarily field galaxies.

4. DISCUSSION

In this paper, we examine the SFHs of quiescent galaxies in an overdensity at $z \sim 2.6$ and find no evidence of environmental quenching in those that reside in an overdense environment as compared to those that reside in the coeval field. We find these subsamples of galaxies have similar formation and quenching times, quenching timescales, stacked SFHs, and sizes across all stellar mass ranges as shown in Figures 3, 4, and 5. Our results suggest that this proto-cluster environment is not efficiently altering the quenching process in galaxies at $z \approx 2.6$.

Our study focuses on comparing the relative ages of low-mass quiescent galaxies in the overdensity and the field. The absolute calibration of galaxy ages – especially mass-weighted ages like those we use here – depend on the choice of SFH priors (e.g., Leja et al. 2019; Suess et al. 2022). Because of this, we refrain from directly comparing our timescale measurements with the various timescales predicted by different quenching mechanisms and other observational studies. We note potential differences in absolute ages between light-weighted ages (e.g., Cutler et al. 2024) and mass-weighted ages (e.g., this Letter) for similar subsamples and refer the reader to a detailed comparison of SFH priors in Gallazzi et al. (in prep.). However, the fact that our measured ages agree for the overdensity and field samples points towards similar quenching mechanisms acting on both populations, unlikely to be environmentally driven. Further observations with medium-resolution spectroscopy could break the age-metallicity degeneracy and improve the absolute calibration of our ages, allowing for more precise comparisons to theoretical predictions.

To further verify our key result that the ages of overdensity and field galaxies are consistent, we show in Figure 6 the positions of our galaxies on the UVJ color-color diagram. Previous work (e.g., Whitaker et al. 2012; Belli et al. 2019) suggests that the location of quiescent galaxies in this color-color space is a good indicator of their age (though metallicity effects are also important, see Cheng et al. (in prep.)) We find that low-mass quiescent galaxies as shown in the left panel of Figure 6 occupy a similar region of the UVJ diagram as the relatively young low-mass quiescent galaxies in Cutler et al. (2024). Figure 6 also shows that the low-mass quiescent galaxies in the overdensity have comparable UVJ colors as low-mass quiescent galaxies in the field suggesting similar SPS properties and ages. These similarities point towards the same conclusion: the quenching mechanisms of

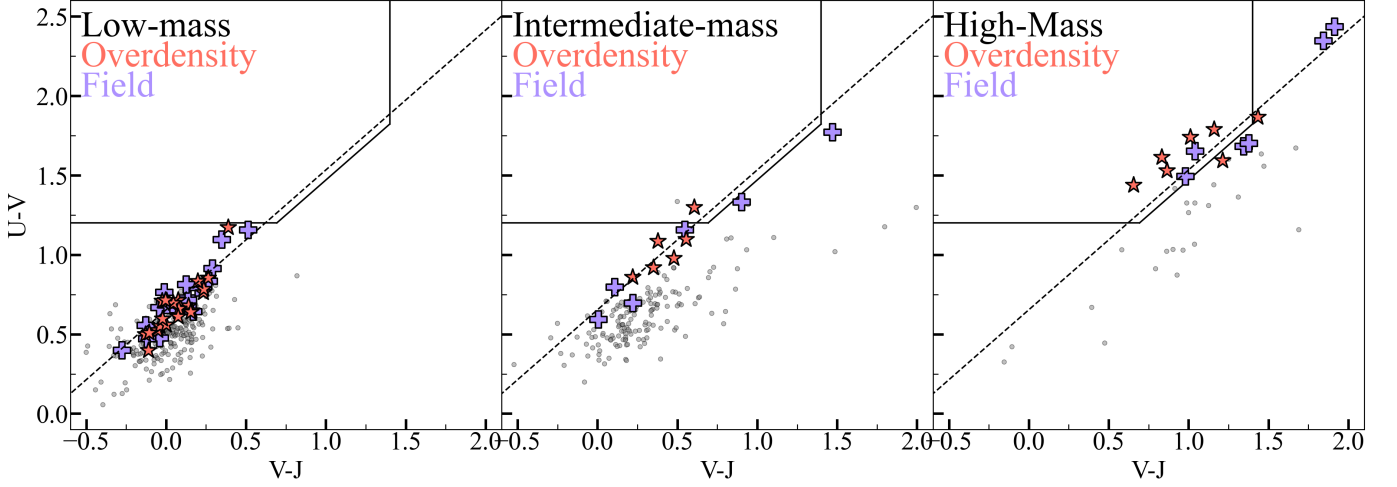


Figure 6. UVJ color-color diagram in the three stellar mass bins. Similarly to Fig. 2, red stars indicate quiescent galaxies in the overdensity, purple crosses indicate quiescent galaxies in the field, and the grey points indicate all other galaxies in the overdensity or field. The solid lines indicate the traditional quiescent wedge from Whitaker et al. (2011) and the solid dashed line indicates the Belli et al. (2019) selection. We find that all low-mass galaxies would otherwise be not selected using the UVJ diagram. There is significant overlap between quiescent galaxies in the overdensity and field suggesting that they have similar SPS properties.

the two samples are likely consistent, and unlikely to be environmentally driven.

Our results are consistent with previous observational studies accessible pre-JWST, which have found no evidence for environmental quenching at cosmic noon (Edward et al. 2024; Singh et al. 2024; Forrest et al. 2024). Edward et al. (2024) and Forrest et al. (2024) argue that the similarity in the quenched fraction of lower-mass ($9.5 < \log(M_*/M_\odot) < 10$) quiescent galaxies in proto-clusters and the field suggests that the proto-cluster environment is not accelerating quenching. This scenario potentially contrasts with the simulation results from Ahad et al. (2024) in which they found that the quenched fraction of similar-mass galaxies in the overdense environment evolves from 0% to 10% from $z \sim 3.5$ to $z \sim 2.0$. While their simulation results are consistent with observations of high-mass galaxies (van der Burg et al. 2020; Webb et al. 2020; Edward et al. 2024; Forrest et al. 2024; Singh et al. 2024), this is not necessarily true for low-mass galaxies and further investigation is needed to reconcile the simulations with the observations.

Potential uncertainties in our study could lead to differing conclusions with the simulation. Associating galaxies with a physical overdensity using photometric redshifts will always be complicated given uncertainties from SED modeling. However, we mitigate this uncertainty by including deep medium band photometry, which we demonstrate provide the necessary average precision for this task ($\sigma_{\text{NMAD}} \sim 0.01 * (1 + z)$, Fig. 1). Future spectroscopic surveys will be critical to ensure complete selection of galaxies in the overdensity, constrain their stellar populations and star-formation histories, and confirm their quiescence. Even still, small extragalactic fields will have limitations with cosmic variance and

constructing truly coeval field samples (i.e., at the same exact redshift). Much larger fields with similar quality data are on the horizon (e.g., Technicolor, GO-3362, PI: Muzzin; JUMPS, GO-5890, PI: Withers; MINERVA, GO-7814, PIs: Marchesini, Muzzin, & Suess; SPAM, GO-8559, PI: Davis) and will provide more stringent tests on the emergence of environmental quenching. Further morphological analysis to determine *where* quenching occurs within galaxies, such as inside-out versus outside-in quenching, is crucial for gaining a deeper understanding of the mechanisms driving quenching in low-mass galaxies (Bezanson et al. 2009; Suess et al. 2019; Alberts & Noble 2022).

Continuing from previous observational works, our current study tells a consistent story: proto-cluster environments at $z \sim 2 - 3$ do not enhance or accelerate quenching compared to the field at an epoch and stellar mass regime (down to $\log(M_*/M_\odot) \sim 8.5$ at $z \sim 2$) which were previously beyond the capabilities of HST or ground-based facilities. This indicates that environmental quenching is not yet playing a primary role in the suppression of star formation of these galaxies at these redshifts potentially due to the lack of a sufficiently dense and hot ICM to effectively strip cold-gas. Eventually, though, environmental quenching will happen as seen in many low- z studies (Dressler 1980; Balogh et al. 2004; Kauffmann et al. 2004; Baldry et al. 2006; Peng et al. 2010b; Muzzin et al. 2014; Hamadouche et al. 2024; Cutler et al. in prep.) and future work will uncover when this happens.

5. ACKNOWLEDGMENTS

This work is based in part on observations made with the NASA/ESA/CSA *James Webb Space Telescope*. The data were obtained from the Mikulski Archive for Space Tele-

scopes at the Space Telescope Science Institute, which is operated by the Association of Universities for Research in Astronomy, Inc., under NASA contract NAS 5-03127 for the JWST. These observations are associated with the JWST Cycle 1 GO program #2561 and Cycle 2 GO program #4111. The JWST data presented in this article were obtained from the Mikulski Archive for Space Telescopes (MAST) at the Space Telescope Science Institute. Support for program JWST-GO-2561 and JWST-GO-4111 was provided by NASA through a grant from the Space Telescope Science Institute, which is operated by the Associations of Universities for Research in Astronomy, Incorporated, under NASA contract NAS5-26555. This research was supported in part by the University of Pittsburgh Center for Research Computing, RRID:SCR_022735, through the resources provided. Specifically, this work used the H2P cluster, which is supported by NSF award number OAC-2117681. Cloud-based data processing and file storage for this work is provided by the AWS Cloud Credits for Research program. The Cosmic Dawn Center is funded by the Danish National Re-

search Foundation (DNRF) under grant #140. The BGU lensing group acknowledges support by grant No. 2020750 from the United States-Israel Binational Science Foundation (BSF) and grant No. 2109066 from the United States National Science Foundation (NSF), by the Israel Science Foundation Grant No. 864/23, and by the Ministry of Science & Technology, Israel. Computations for this research were performed on the Pennsylvania State University's Institute for Computational and Data Sciences' Roar supercomputer.

Facilities: JWST (NIRSpec, NIRCам), HST (ACS, WFC3)

Software: ASTROPY (Astropy Collaboration et al. 2022), MSAEXP (v0.8.5; (Brammer 2022)), jwst pipeline (v1.14.0; (Bushouse et al. 2022)), GRIZLI (Brammer et al. 2008, github.com/gbrammer/grizli), EAzY (Brammer et al. 2008), MATPLOTLIB (Hunter 2007), NUMPY (van der Walt et al. 2011), DYNASTY (Speagle 2020), PROSPECTOR (Johnson et al. 2021)

REFERENCES

- Ahad, S. L., Muzzin, A., Bahé, Y. M., & Hoekstra, H. 2024, MNRAS, 528, 6329, doi: [10.1093/mnras/stae341](https://doi.org/10.1093/mnras/stae341)
- Alberts, S., & Noble, A. 2022, Universe, 8, 554, doi: [10.3390/universe8110554](https://doi.org/10.3390/universe8110554)
- Alberts, S., Williams, C. C., Helton, J. M., et al. 2024, ApJ, 975, 85, doi: [10.3847/1538-4357/ad66cc](https://doi.org/10.3847/1538-4357/ad66cc)
- Astropy Collaboration, Price-Whelan, A. M., Lim, P. L., et al. 2022, ApJ, 935, 167, doi: [10.3847/1538-4357/ac7c74](https://doi.org/10.3847/1538-4357/ac7c74)
- Baldry, I. K., Balogh, M. L., Bower, R. G., et al. 2006, MNRAS, 373, 469, doi: [10.1111/j.1365-2966.2006.11081.x](https://doi.org/10.1111/j.1365-2966.2006.11081.x)
- Balogh, M. L., Baldry, I. K., Nichol, R., et al. 2004, ApJL, 615, L101, doi: [10.1086/426079](https://doi.org/10.1086/426079)
- Bell, E. F., & de Jong, R. S. 2001, ApJ, 550, 212, doi: [10.1086/319728](https://doi.org/10.1086/319728)
- Belli, S., Newman, A. B., & Ellis, R. S. 2019, ApJ, 874, 17, doi: [10.3847/1538-4357/ab07af](https://doi.org/10.3847/1538-4357/ab07af)
- Bezanson, R., van Dokkum, P. G., Tal, T., et al. 2009, ApJ, 697, 1290, doi: [10.1088/0004-637X/697/2/1290](https://doi.org/10.1088/0004-637X/697/2/1290)
- Bezanson, R., Labbe, I., Whitaker, K. E., et al. 2024, ApJ, 974, 92, doi: [10.3847/1538-4357/ad66cf](https://doi.org/10.3847/1538-4357/ad66cf)
- Boselli, A., Fossati, M., & Sun, M. 2022, A&A Rv, 30, 3, doi: [10.1007/s00159-022-00140-3](https://doi.org/10.1007/s00159-022-00140-3)
- Boselli, A., & Gavazzi, G. 2014, A&A Rv, 22, 74, doi: [10.1007/s00159-014-0074-y](https://doi.org/10.1007/s00159-014-0074-y)
- Brammer, G. 2022, msaexp: NIRSpec analysis tools, 0.4, Zenodo, doi: [10.5281/zenodo.7579050](https://doi.org/10.5281/zenodo.7579050)
- Brammer, G. B., van Dokkum, P. G., & Coppi, P. 2008, ApJ, 686, 1503, doi: [10.1086/591786](https://doi.org/10.1086/591786)
- Bushouse, H., Eisenhamer, J., Dencheva, N., et al. 2022, JWST Calibration Pipeline, 1.14.0, Zenodo, doi: [10.5281/zenodo.7229890](https://doi.org/10.5281/zenodo.7229890)
- Carlsten, S. G., Greene, J. E., Greco, J. P., Beaton, R. L., & Kado-Fong, E. 2021, ApJ, 922, 267, doi: [10.3847/1538-4357/ac2581](https://doi.org/10.3847/1538-4357/ac2581)
- Chabrier, G. 2003, PASP, 115, 763, doi: [10.1086/376392](https://doi.org/10.1086/376392)
- Chen, W., Kelly, P. L., Frye, B. L., et al. 2024, ApJ, 970, 102, doi: [10.3847/1538-4357/ad50a5](https://doi.org/10.3847/1538-4357/ad50a5)
- Chiang, Y.-K., Overzier, R., & Gebhardt, K. 2013, ApJ, 779, 127, doi: [10.1088/0004-637X/779/2/127](https://doi.org/10.1088/0004-637X/779/2/127)
- Chiang, Y.-K., Overzier, R. A., Gebhardt, K., & Henriques, B. 2017, ApJL, 844, L23, doi: [10.3847/2041-8213/aa7e7b](https://doi.org/10.3847/2041-8213/aa7e7b)
- Ciotti, L., D'Ercole, A., Pellegrini, S., & Renzini, A. 1991, ApJ, 376, 380, doi: [10.1086/170289](https://doi.org/10.1086/170289)
- Cortese, L., Catinella, B., & Smith, R. 2021, PASA, 38, e035, doi: [10.1017/pasa.2021.18](https://doi.org/10.1017/pasa.2021.18)
- Croton, D. J., Springel, V., White, S. D. M., et al. 2006, MNRAS, 365, 11, doi: [10.1111/j.1365-2966.2005.09675.x](https://doi.org/10.1111/j.1365-2966.2005.09675.x)
- Crowl, H. H., & Kenney, J. D. P. 2008, AJ, 136, 1623, doi: [10.1088/0004-6256/136/4/1623](https://doi.org/10.1088/0004-6256/136/4/1623)
- Cutler, S. E., Whitaker, K. E., Mowla, L. A., et al. 2022, ApJ, 925, 34, doi: [10.3847/1538-4357/ac341c](https://doi.org/10.3847/1538-4357/ac341c)
- Cutler, S. E., Whitaker, K. E., Weaver, J. R., et al. 2024, ApJL, 967, L23, doi: [10.3847/2041-8213/ad464c](https://doi.org/10.3847/2041-8213/ad464c)
- Dressler, A. 1980, ApJ, 236, 351, doi: [10.1086/157753](https://doi.org/10.1086/157753)
- Edward, A. H., Balogh, M. L., Bahé, Y. M., et al. 2024, MNRAS, 527, 8598, doi: [10.1093/mnras/stad3751](https://doi.org/10.1093/mnras/stad3751)

- Farouki, R., & Shapiro, S. L. 1981, *ApJ*, 243, 32, doi: [10.1086/158563](https://doi.org/10.1086/158563)
- Forrest, B., Lemaux, B. C., Shah, E. A., et al. 2024, *ApJ*, 971, 169, doi: [10.3847/1538-4357/ad5e78](https://doi.org/10.3847/1538-4357/ad5e78)
- Furtak, L. J., Zitrin, A., Weaver, J. R., et al. 2023, *MNRAS*, 523, 4568, doi: [10.1093/mnras/stad1627](https://doi.org/10.1093/mnras/stad1627)
- Gunn, J. E., & Gott, J. Richard, I. 1972, *ApJ*, 176, 1, doi: [10.1086/151605](https://doi.org/10.1086/151605)
- Hamadouche, M. L., McLure, R. J., Carnall, A., et al. 2024, arXiv e-prints, arXiv:2412.09592, doi: [10.48550/arXiv.2412.09592](https://doi.org/10.48550/arXiv.2412.09592)
- Hinshaw, G., Larson, D., Komatsu, E., et al. 2013, *ApJS*, 208, 19, doi: [10.1088/0067-0049/208/2/19](https://doi.org/10.1088/0067-0049/208/2/19)
- Hoffman, M. D., & Gelman, A. 2014, *Journal of Machine Learning Research*, 15, 1593. <http://jmlr.org/papers/v15/hoffman14a.html>
- Hunter, J. D. 2007, *CSE*, 9, 90, doi: [10.1109/MCSE.2007.55](https://doi.org/10.1109/MCSE.2007.55)
- Ishibashi, W., & Fabian, A. C. 2012, *MNRAS*, 427, 2998, doi: [10.1111/j.1365-2966.2012.22074.x](https://doi.org/10.1111/j.1365-2966.2012.22074.x)
- Johnson, B. D., Leja, J., Conroy, C., & Speagle, J. S. 2021, *ApJS*, 254, 22, doi: [10.3847/1538-4365/abef67](https://doi.org/10.3847/1538-4365/abef67)
- Kauffmann, G., White, S. D. M., Heckman, T. M., et al. 2004, *MNRAS*, 353, 713, doi: [10.1111/j.1365-2966.2004.08117.x](https://doi.org/10.1111/j.1365-2966.2004.08117.x)
- Kawinwanichakij, L., Quadri, R. F., Papovich, C., et al. 2016, *ApJ*, 817, 9, doi: [10.3847/0004-637X/817/1/9](https://doi.org/10.3847/0004-637X/817/1/9)
- Kawinwanichakij, L., Papovich, C., Quadri, R. F., et al. 2017, *ApJ*, 847, 134, doi: [10.3847/1538-4357/aa8b75](https://doi.org/10.3847/1538-4357/aa8b75)
- Kuchner, U., Ziegler, B., Verdugo, M., Bamford, S., & Häußler, B. 2017, *A&A*, 604, A54, doi: [10.1051/0004-6361/201630252](https://doi.org/10.1051/0004-6361/201630252)
- Leja, J., Speagle, J. S., Johnson, B. D., et al. 2020, *ApJ*, 893, 111, doi: [10.3847/1538-4357/ab7e27](https://doi.org/10.3847/1538-4357/ab7e27)
- Leja, J., Johnson, B. D., Conroy, C., et al. 2019, *ApJ*, 877, 140, doi: [10.3847/1538-4357/ab1d5a](https://doi.org/10.3847/1538-4357/ab1d5a)
- Leja, J., Speagle, J. S., Ting, Y.-S., et al. 2022, *ApJ*, 936, 165, doi: [10.3847/1538-4357/ac887d](https://doi.org/10.3847/1538-4357/ac887d)
- Li, Z., Cai, Z., Sun, F., et al. 2023, arXiv e-prints, arXiv:2310.09327, doi: [10.48550/arXiv.2310.09327](https://doi.org/10.48550/arXiv.2310.09327)
- Lotz, J. M., Koekemoer, A., Coe, D., et al. 2017, *ApJ*, 837, 97, doi: [10.3847/1538-4357/837/1/97](https://doi.org/10.3847/1538-4357/837/1/97)
- Man, A., & Belli, S. 2018, *Nature Astronomy*, 2, 695, doi: [10.1038/s41550-018-0558-1](https://doi.org/10.1038/s41550-018-0558-1)
- Marchesini, D., Brammer, G., Morishita, T., et al. 2023, *ApJL*, 942, L25, doi: [10.3847/2041-8213/acaac](https://doi.org/10.3847/2041-8213/acaac)
- McNab, K., Balogh, M. L., van der Burg, R. F. J., et al. 2021, *MNRAS*, 508, 157, doi: [10.1093/mnras/stab2558](https://doi.org/10.1093/mnras/stab2558)
- Mérida, R. M., Pérez-González, P. G., Sánchez-Blázquez, P., et al. 2023, *ApJ*, 950, 125, doi: [10.3847/1538-4357/acc7a3](https://doi.org/10.3847/1538-4357/acc7a3)
- Miller, T. B., Suess, K. A., Setton, D. J., et al. 2024, arXiv e-prints, arXiv:2412.06957, doi: [10.48550/arXiv.2412.06957](https://doi.org/10.48550/arXiv.2412.06957)
- Moore, B., Katz, N., Lake, G., Dressler, A., & Oemler, A. 1996, *Nature*, 379, 613, doi: [10.1038/379613a0](https://doi.org/10.1038/379613a0)
- Muldrew, S. I., Hatch, N. A., & Cooke, E. A. 2015, *MNRAS*, 452, 2528, doi: [10.1093/mnras/stv1449](https://doi.org/10.1093/mnras/stv1449)
- Muzzin, A., van der Burg, R. F. J., McGee, S. L., et al. 2014, *ApJ*, 796, 65, doi: [10.1088/0004-637X/796/1/65](https://doi.org/10.1088/0004-637X/796/1/65)
- Naidu, R. P., Matthee, J., Kramarenko, I., et al. 2024, arXiv e-prints, arXiv:2410.01874, doi: [10.48550/arXiv.2410.01874](https://doi.org/10.48550/arXiv.2410.01874)
- Nedkova, K. V., Häußler, B., Marchesini, D., et al. 2021, *MNRAS*, 506, 928, doi: [10.1093/mnras/stab1744](https://doi.org/10.1093/mnras/stab1744)
- Overzier, R. A. 2016, *A&A Rv*, 24, 14, doi: [10.1007/s00159-016-0100-3](https://doi.org/10.1007/s00159-016-0100-3)
- Papovich, C., Kawinwanichakij, L., Quadri, R. F., et al. 2018, *ApJ*, 854, 30, doi: [10.3847/1538-4357/aaa766](https://doi.org/10.3847/1538-4357/aaa766)
- Pasha, I., & Miller, T. B. 2023, *The Journal of Open Source Software*, 8, 5703, doi: [10.21105/joss.05703](https://doi.org/10.21105/joss.05703)
- Paulino-Afonso, A., Sobral, D., Darvish, B., et al. 2020, *A&A*, 633, A70, doi: [10.1051/0004-6361/201834244](https://doi.org/10.1051/0004-6361/201834244)
- Peng, C. Y., Ho, L. C., Impey, C. D., & Rix, H.-W. 2002, *AJ*, 124, 266, doi: [10.1086/340952](https://doi.org/10.1086/340952)
- , 2010a, *AJ*, 139, 2097, doi: [10.1088/0004-6256/139/6/2097](https://doi.org/10.1088/0004-6256/139/6/2097)
- Peng, Y., Maiolino, R., & Cochrane, R. 2015, *Nature*, 521, 192, doi: [10.1038/nature14439](https://doi.org/10.1038/nature14439)
- Peng, Y.-j., Lilly, S. J., Kovač, K., et al. 2010b, *ApJ*, 721, 193, doi: [10.1088/0004-637X/721/1/193](https://doi.org/10.1088/0004-637X/721/1/193)
- Phan, D., Pradhan, N., & Jankowiak, M. 2019, arXiv e-prints, arXiv:1912.11554, doi: [10.48550/arXiv.1912.11554](https://doi.org/10.48550/arXiv.1912.11554)
- Price, S. H., Bezanson, R., Labbe, I., et al. 2024, arXiv e-prints, arXiv:2408.03920, doi: [10.48550/arXiv.2408.03920](https://doi.org/10.48550/arXiv.2408.03920)
- Renzini, A. 2006, *ARA&A*, 44, 141, doi: [10.1146/annurev.astro.44.051905.092450](https://doi.org/10.1146/annurev.astro.44.051905.092450)
- Rodríguez Montero, F., Davé, R., Wild, V., Anglés-Alcázar, D., & Narayanan, D. 2019, *MNRAS*, 490, 2139, doi: [10.1093/mnras/stz2580](https://doi.org/10.1093/mnras/stz2580)
- Sarazin, C. L. 1986, *Reviews of Modern Physics*, 58, 1, doi: [10.1103/RevModPhys.58.1](https://doi.org/10.1103/RevModPhys.58.1)
- Singh, A., Guaita, L., Hibon, P., et al. 2024, arXiv e-prints, arXiv:2411.12722, doi: [10.48550/arXiv.2411.12722](https://doi.org/10.48550/arXiv.2411.12722)
- Speagle, J. S. 2020, *MNRAS*, 493, 3132, doi: [10.1093/mnras/staa278](https://doi.org/10.1093/mnras/staa278)
- Steinhardt, C. L., Jauzac, M., Acebron, A., et al. 2020, *ApJS*, 247, 64, doi: [10.3847/1538-4365/ab75ed](https://doi.org/10.3847/1538-4365/ab75ed)
- Steinhauser, D., Schindler, S., & Springel, V. 2016, *A&A*, 591, A51, doi: [10.1051/0004-6361/201527705](https://doi.org/10.1051/0004-6361/201527705)
- Suess, K. A., Kriek, M., Price, S. H., & Barro, G. 2019, *ApJ*, 877, 103, doi: [10.3847/1538-4357/ab1bda](https://doi.org/10.3847/1538-4357/ab1bda)
- Suess, K. A., Leja, J., Johnson, B. D., et al. 2022, *ApJ*, 935, 146, doi: [10.3847/1538-4357/ac82b0](https://doi.org/10.3847/1538-4357/ac82b0)
- Suess, K. A., Weaver, J. R., Price, S. H., et al. 2024, arXiv e-prints, arXiv:2404.13132, doi: [10.48550/arXiv.2404.13132](https://doi.org/10.48550/arXiv.2404.13132)
- Tal, T., Dekel, A., Oesch, P., et al. 2014, *ApJ*, 789, 164, doi: [10.1088/0004-637X/789/2/164](https://doi.org/10.1088/0004-637X/789/2/164)

- Thomas, D., Maraston, C., Bender, R., & Mendes de Oliveira, C. 2005, *ApJ*, 621, 673, doi: [10.1086/426932](https://doi.org/10.1086/426932)
- Thomas, D., Maraston, C., Schawinski, K., Sarzi, M., & Silk, J. 2010, *MNRAS*, 404, 1775, doi: [10.1111/j.1365-2966.2010.16427.x](https://doi.org/10.1111/j.1365-2966.2010.16427.x)
- Tomczak, A. R., Lemaux, B. C., Lubin, L. M., et al. 2017, *MNRAS*, 472, 3512, doi: [10.1093/mnras/stx2245](https://doi.org/10.1093/mnras/stx2245)
- Trager, S. C., Faber, S. M., Worthey, G., & González, J. J. 2000, *AJ*, 120, 165, doi: [10.1086/301442](https://doi.org/10.1086/301442)
- Treu, T., Roberts-Borsani, G., Bradac, M., et al. 2022, *ApJ*, 935, 110, doi: [10.3847/1538-4357/ac8158](https://doi.org/10.3847/1538-4357/ac8158)
- van der Burg, R. F. J., Rudnick, G., Balogh, M. L., et al. 2020, *A&A*, 638, A112, doi: [10.1051/0004-6361/202037754](https://doi.org/10.1051/0004-6361/202037754)
- van der Walt, S., Colbert, S. C., & Varoquaux, G. 2011, *CSE*, 13, 22, doi: [10.1109/MCSE.2011.37](https://doi.org/10.1109/MCSE.2011.37)
- van Dokkum, P. G., & Stanford, S. A. 2003, *ApJ*, 585, 78, doi: [10.1086/345989](https://doi.org/10.1086/345989)
- Wang, B., Leja, J., Bezanson, R., et al. 2023, *ApJL*, 944, L58, doi: [10.3847/2041-8213/acba99](https://doi.org/10.3847/2041-8213/acba99)
- Wang, B., Leja, J., Labbé, I., et al. 2024, *ApJS*, 270, 12, doi: [10.3847/1538-4365/ad0846](https://doi.org/10.3847/1538-4365/ad0846)
- Weaver, J. R., Cutler, S. E., Pan, R., et al. 2024, *ApJS*, 270, 7, doi: [10.3847/1538-4365/ad07e0](https://doi.org/10.3847/1538-4365/ad07e0)
- Webb, K., Balogh, M. L., Leja, J., et al. 2020, *MNRAS*, 498, 5317, doi: [10.1093/mnras/staa2752](https://doi.org/10.1093/mnras/staa2752)
- Whitaker, K. E., Kriek, M., van Dokkum, P. G., et al. 2012, *ApJ*, 745, 179, doi: [10.1088/0004-637X/745/2/179](https://doi.org/10.1088/0004-637X/745/2/179)
- Whitaker, K. E., Labbé, I., van Dokkum, P. G., et al. 2011, *ApJ*, 735, 86, doi: [10.1088/0004-637X/735/2/86](https://doi.org/10.1088/0004-637X/735/2/86)
- Whitaker, K. E., Franx, M., Leja, J., et al. 2014, *ApJ*, 795, 104, doi: [10.1088/0004-637X/795/2/104](https://doi.org/10.1088/0004-637X/795/2/104)